

RIFE: Real-Time Intermediate Flow Estimation for Video Frame Interpolation

Zhewei Huang¹ Tianyuan Zhang¹ Wen Heng¹ Boxin Shi² Shuchang Zhou¹
¹Megvii Inc ²Peking University

{huangzhewei, zhangtianyuan, hengwen, zsc}@megvii.com, shiboxin@pku.edu.cn

Abstract

We propose RIFE, a Real-time Intermediate Flow Estimation algorithm for Video Frame Interpolation (VFI). Most existing flow-based methods first estimate the bi-directional optical flows, then scale and reverse them to approximate intermediate flows, leading to artifacts on motion boundaries. RIFE uses a neural network named IFNet that can directly estimate the intermediate flows from images with much better speed. Based on our proposed leakage distillation loss, RIFE can be trained in an end-to-end fashion. Experiments demonstrate that our method is flexible and can achieve impressive performance on several public benchmarks. The code is available at <https://github.com/hzwer/arXiv2020-RIFE>

1. Introduction

Video Frame Interpolation (VFI) aims to synthesize intermediate frames between two consecutive frames of a video and is widely used to improve frame rate and enhance visual quality. VFI also supports various applications like slow-motion generation, video compression [34], and novel view rendering. Moreover, real-time VFI algorithms running on high-resolution videos have many more potential applications, such as increasing the frame rate of video games and live videos, providing video editing services for users with limited computing resources.

VFI is challenging due to the complex, large non-linear motions and illumination changes in the real world. Recently, flow-based VFI algorithms have offered a framework to address these challenges and achieved impressive results [13, 24, 37, 2]. Common approaches for these methods involve two steps: 1) warping the input frames according to approximated optical flows and 2) fusing and refining the warped frames using a bunch of Convolutional Neural Networks (CNNs).

According to the way of warping frames, flow-based VFI algorithms can be classified into forward warping based methods and backward warping based methods. Backward warping is more widely used because forward warp-

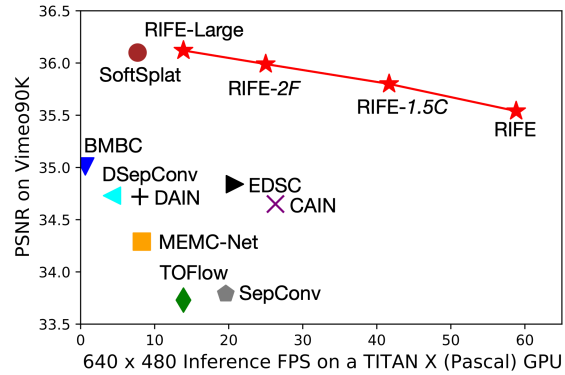


Figure 1: **Speed and accuracy trade-off by adjusting model size parameters C and F .** We compare our models with prior VFI methods including TOFlow [37], SepConv [27], MEMC-Net [3], DAIN [2], CAIN [7], SoftSplat [25], BMBC [28], DSepConv [6], and EDSC [5] on the Vimeo90K testing set.

ing suffers from conflicts when multiple source pixels are mapped to the same location, leading to overlapped pixels and holes. Given the input frames I_0, I_1 , backward warping based methods need to approximate the intermediate flows $F_{t \rightarrow 0}, F_{t \rightarrow 1}$ from the perspective of the frame I_t that we are expected to synthesize. Common practices [13, 2, 36, 18] first compute bi-directional flows from pre-trained off-the-shelf optical flow models, then reverse and refine them to generate intermediate flows. However, these methods may have flaws on motion boundaries, as the object position changes from frame to frame. Consequently, previous VFI methods share two major drawbacks:

- 1) Requiring additional components: Image depth [2], flow refinement [13] and flow reversal layer [36, 18] are introduced to compensate for the defects of optical flow reversal. These operations require a large amount computing resources and are not suitable for real-time scenarios.
- 2) Having no direct supervision for the approximated intermediate flows: The whole interpolation system is usually trained with only the final reconstruction loss [28]. There is no other supervision explicitly designed for the

flow estimation process, degrading the performance of interpolation.

We develop a specialized intermediate flow network named **IFNet** to directly estimate the intermediate flows. IFNet adopts a coarse-to-fine strategy [12] with progressively increased resolutions: it iteratively updates a flow field via successive IFBlocks. Conceptually, according to the iteratively updated flow fields, we move corresponding pixels from two input frames to the same location in a latent intermediate frame. Unlike most previous optical flow models [8, 12, 32, 11, 33], IFBlocks do not contain expensive operators like cost volume or pyramid feature warping and use 3×3 convolution as building blocks.

IFNet can be trained end-to-end with a later fusion process using only the final reconstruction loss, like existing works [19, 28] that estimate the intermediate flow directly from images without proper supervision for intermediate flows. In line with intuition, our method produces worse results than previous methods that use complex pipelines and pre-trained flow models in the intermediate flow estimation process. However, the picture dramatically changes after we add advanced supervisions to IFNet. We design a census loss adapted from unsupervised optical flow learning [22, 15] and a novel leakage distillation loss. This distillation loss employs an overpowered teacher with access to the intermediate frames during training. Combining these designs, we propose Realtime Intermediate Flow Estimation (**RIFE**). RIFE can achieve satisfactory results when trained from scratch. We illustrate the speed and accuracy trade-off compared with other methods in Figure 1.

In summary, our contributions are three-fold:

- We design an efficient IFNet to simplify the flow-based VFI methods. IFNet can be trained from scratch and directly approximate the intermediate flows given two input frames.
- We provide effective supervision for intermediate flow estimation by proposing an adapted census loss and a leakage distillation loss, which leads to a more stable convergence and large performance improvement.
- We use model scaling to obtain models with varying quality and speed trade-offs. Experiments show that RIFE can achieve impressive performance on public benchmarks.

2. Related Work

We provide a brief overview of the optical flow estimation task, which is the core of most VFI methods. Then, we will review several most related flow-based VFI methods, and cover some inspiring flow-free methods.

2.1. Optical Flow

Optical flow estimation is a long-standing vision task that aims to estimate the per-pixel motion, which can be used in lots of downstream tasks. Since the milestone work of FlowNet [8] based on U-net autoencoder [30], architectures for optical flow models have evolved for several years, yielding more accurate results while being more efficient, such as FlowNet2 [12], PWC-Net [32] and LiteFlowNet [11]. These methods typically adopt an iterative refinement approach and often involve operators like cost volume, pyramidal features, and backward feature warping. Recently Teed *et al.* [33] introduce RAFT, which iteratively updates a flow field through a recurrent unit and achieves a remarkable breakthrough in this field. Another important research direction is unsupervised optical flow estimation [22, 15, 21] due to the difficulty of optical flow labeling.

2.2. Video Frame Interpolation

Most previous methods are designed for interpolating intermediate frames using only two reference frames. Specifically, Liu *et al.* [19] propose a fully convolutional network to estimate voxel flow and generate intermediate frames by sampling. Jiang *et al.* [13] propose SuperSloMo using the linear combination of the two bi-directional flows as an initial approximation of the intermediate flows. Then refine them and predict visibility maps that encode occlusion information. Based on SuperSloMo, Reda *et al.* [29] propose to synthesize intermediate frames using unsupervised cycle consistency. Bao *et al.* [2] propose DAIN using a depth-aware flow projection layer to estimate the intermediate flow as a weighted combination of bidirectional flow. Niklaus *et al.* [25] propose SoftSplat to forward-warp frames and their feature map using softmax splatting. Xu *et al.* [36] propose QVI to exploit four consecutive frames and flow reversal filter to get the intermediate flows. Liu *et al.* [18] further extend QVI with rectified quadratic flow prediction to EQVI. Among these methods, DAIN has been deployed in many software applications, and SoftSplat leads in many public benchmarks.

Along with flow-based methods, flow-free methods have also achieved remarkable progress in recent years. Meyer *et al.* [23] utilize phase information to learn the motion relationship for multiple video frame interpolation. Niklaus *et al.* [26, 27] formulate VFI as a spatially-adaptive convolution whose convolution kernel is generated using a convolution network given the input frames. Cheng *et al.* propose DSepConv [6] to extend kernel-based method using deformable separable convolution and further propose EDSC [5] to perform multiple interpolation. Choi *et al.* [7] propose an efficient flow-free method named CAIN, which employs the PixelShuffle operator and channel attention to capture the motion information implicitly.

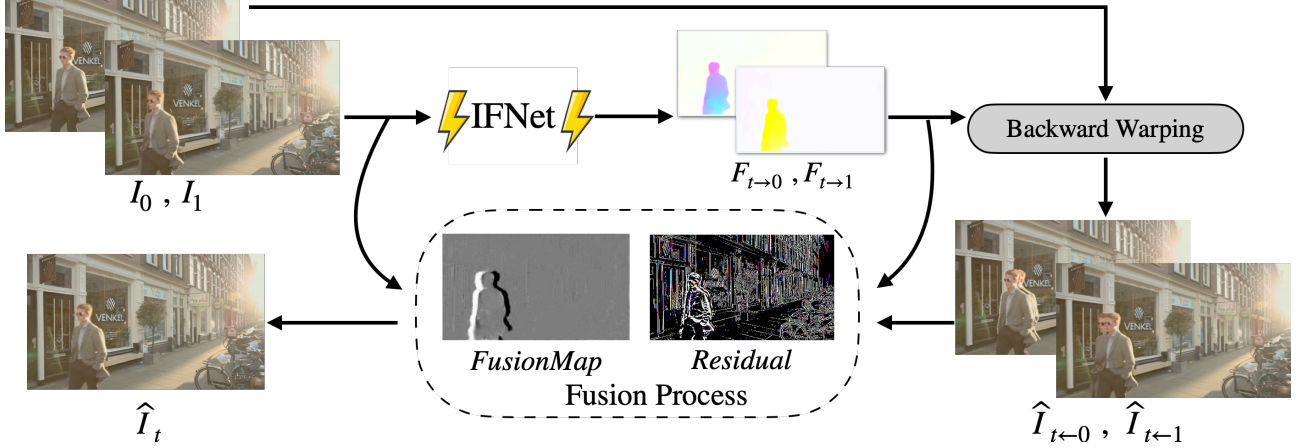


Figure 2: **Overview of RIFE.** Given two input frames I_0, I_1 , we directly feed them into our efficient IFNet to approximate intermediate flows $F_{t \rightarrow 0}, F_{t \rightarrow 1}$. The fusion process takes the warped frames $\hat{I}_{t \leftarrow 0}, \hat{I}_{t \leftarrow 1}$, intermediate flows $F_{t \rightarrow 0}, F_{t \rightarrow 1}$ and the input frames I_0, I_1 as input. Inside the fusion process, a FusionMap and Residual is firstly estimated, then the warped frames are linearly combined according to the FusionMap, and added with the Residual to reconstruct the frame \hat{I}_t .

3. Method

In this section, we first provide an overview of our proposed RIFE. We then describe the efficient design of the major components in RIFE in section 3.2, elaborate on our proposed leakage distillation loss in section 3.3, and explain the training details in section 3.4.

3.1. Pipeline Overview

We illustrate the overview of our proposed RIFE in Figure 2. Given a pair of consecutive RGB frames, I_0, I_1 , our goal is to synthesize an intermediate frame \hat{I}_t at time $t = 0.5$. We directly estimate the intermediate flows $F_{t \rightarrow 0}$ and $F_{t \rightarrow 1}$ by feeding input frames into IFNet. Then we can get two coarse results $\hat{I}_{t \leftarrow 0}, \hat{I}_{t \leftarrow 1}$ by backward warping the input frames. To remove the artifacts in the warped frames, we feed the input frames, the approximated flow, and warped frames into the fusion process with an encoder-decoder like FusionNet to generate the final result.

3.2. Efficient Architecture Design

RIFE has two major components: 1) efficient *intermediate flow estimation* with the IFNet and 2) **fusion Process** of the warped frames. We describe the details of these components in this subsection.

Intermediate flow estimation. Some previous intermediate flow estimation methods need to reverse and refine bi-directional flows [13, 36, 2, 18] as depicted in Figure 3. The role of our IFNet is to directly and efficiently predict $F_{t \rightarrow 0}, F_{t \rightarrow 1}$ given two consecutive input frames I_0, I_1 .

To handle the large motion encountered in intermediate flow estimation, we employ a coarse-to-fine strategy with gradually increasing resolutions. We illustrate the detailed

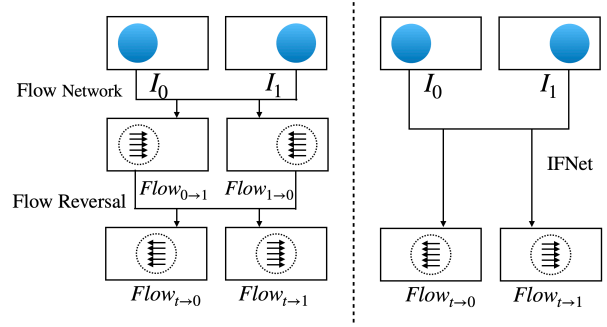


Figure 3: **Comparison between previous intermediate estimation approaches [13, 36, 2, 18] (left) and IFNet (right).** Existing methods are composed of two stages: 1) bi-direction flow estimation and 2) flow reversal. IFNet can directly estimate the intermediate flows.

architecture of IFNet in Figure 4. Specifically, we first compute a rough prediction of the flow on low resolutions, which is believed to capture large motions easier, then iteratively refine the flow fields with gradually increasing resolutions. Following this design, our IFNet has a stacked hour-glass structure, where a flow field is iteratively refined via successive IFBlocks operating on increasing resolutions:

$$F^i = F^{i-1} + g^i(F^{i-1}, \hat{I}^{i-1}), \quad (1)$$

where F^{i-1} denotes the current estimation of the intermediate flows from the $i - 1$ -th IFBlock, $\hat{I}_{0 \rightarrow t}^{i-1}$ and $\hat{I}_{1 \rightarrow t}^{i-1}$ denote the warped input frames using previous approximated flow, and g^i represents the i th IFBlock. We use a total of 3 IFBlocks, and each has a resolution parameter, K_i . To keep our design simple, each IFBlock has a feed-forward structure consisting of several convolutional layers and an

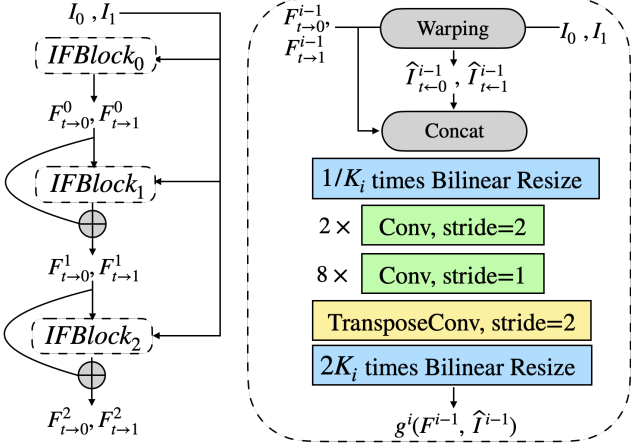


Figure 4: **Structure of IFNet.** **Left:** IFNet is composed of three stacked IFBlocks operating at different resolutions. **Right:** We firstly warp the two input frames based on current approximated flow F^{i-1} . Then the warped frames \hat{I}^{i-1} and F^{i-1} are fed into the next IFBlock to approximate a flow residual.

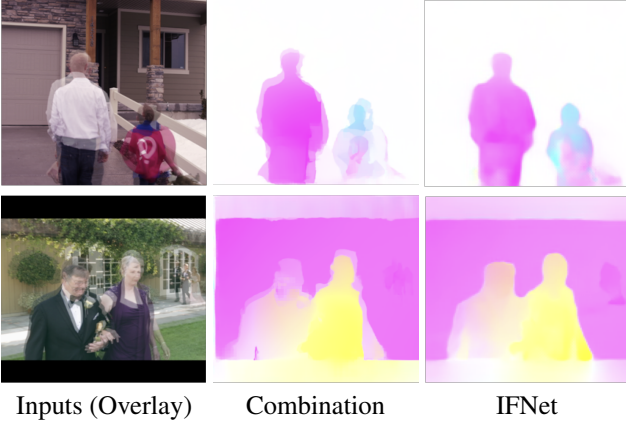


Figure 5: **Visual comparison between linearly combined bi-directional flows generated by a pre-trained LiteFlowNet [11] and the intermediate flow approximated by IFNet.** IFNet produces clear motion boundaries.

up-sampling operator. Except for the layer that outputs the optical flow residuals, the fusion map, and the reconstruction residual, we use PReLU [9] as the activation function.

In Figure 5, we provide visual results of our IFNet and compare them with the linearly combined bi-directional optical flows generated by a pre-trained LiteFlowNet [11]. Our IFNet produces clear and sharp motion boundaries, while linearly combined flow suffers from overlapped pixels and blurring on motion boundaries.

We compare the runtime of the current state-of-the-art optical flow estimation networks [32, 11, 12] and our IFNet in Table 1. Current flow-based models usually need to be

Table 1: **Inference time on 720p video.** Standard flow-based VFI methods run the flow estimation network twice to obtain bi-directional optical flows.

Method	PWC-Net	LiteFlowNet	FlowNet2	IFNet
Runtime	$2 \times 52\text{ms}$	$2 \times 152\text{ms}$	$2 \times 207\text{ms}$	17ms

run twice to get the bi-directional flows. Thus our intermediate flow estimation process runs around 5–20 times faster than previous methods.

Fusion process. With the estimated intermediate flows $F_{t \rightarrow 0}, F_{t \rightarrow 1}$, we can get the coarse reconstruction $\hat{I}_{t \leftarrow 0}, \hat{I}_{t \leftarrow 1}$ by performing backward warping on input frames. To reduce the severe artifacts in the warped frames, we perform a refine and fusion process formulated as:

$$\hat{I}_t = M \odot \hat{I}_{t \leftarrow 0} + (1 - M) \odot \hat{I}_{t \leftarrow 1} + \Delta, \quad (2)$$

where M is a soft fusion map used to fuse the two warped frames, Δ is the reconstruction residual term used to refine the details in images, \odot is an element-wise multiplier, and $(0 \leq M, \Delta \leq 1)$.

Following previous work [13, 2, 25], the fusion process includes a context extractor and a FusionNet with an encoder-decoder architecture similar to U-Net. The context extractor and encoder part of the FusionNet have similar architectures, consisting of four convolutional blocks, and each of the convolutional blocks is composed of two 3×3 convolutional layers, respectively. The decoder part in the FusionNet has four transpose convolution layers. We use sigmoid function to restrict the outputs of FusionNet.

Specifically, the context extractor first extracts the pyramid contextual features from input frames separately. We denote the pyramid contextual feature as C_0 : $\{C_0^0, C_0^1, C_0^2, C_0^3\}$ and C_1 : $\{C_1^0, C_1^1, C_1^2, C_1^3\}$. We then perform backward warping on these features using estimated intermediate flows to produce aligned pyramid features, $C_{t \leftarrow 0}$ and $C_{t \leftarrow 1}$. The warped frames and intermediate flows are fed into the FusionNet, including an encoder and a decoder. The output of i -th encoder block is concatenated with the $C_{t \leftarrow 0}^i$ and $C_{t \leftarrow 1}^i$ before being fed into the next block. The decoder parts finally produce the fusion map M and the reconstruction residual Δ .

3.3. Leakage Distillation for IFNet

Directly approximating the intermediate flows is hard because of no access to the intermediate frame and the lack of supervision. To address this problem, we add a leakage distillation loss to our IFNet in which the target is the prediction of an overpowered teacher network who has access to the intermediate frame. Specifically, we feed $\{I_t^{GT}, I_0\}, \{I_t^{GT}, I_1\}$ to a pre-trained optical flow estimation network to get the intermediate flow prediction

$\{F_{t \rightarrow 1}^{Leak}, F_{t \rightarrow 0}^{Leak}\}$. And the leakage distillation loss \mathcal{L}_{dis} is defined as follows:

$$\mathcal{L}_{dis} = \|F_{t \rightarrow 0} - F_{t \rightarrow 0}^{Leak}\|_1 + \|F_{t \rightarrow 1} - F_{t \rightarrow 1}^{Leak}\|_1. \quad (3)$$

Following previous work [33], we apply the leakage distillation loss over the full sequence of predictions generated from the iteratively updating process in our IFNet.

Our distillation scheme is different from those in semi-supervised learning algorithms [4, 35], where a pre-trained model is used to infer the label of unlabeled data. With the access of the target frame I_t^{GT} , our teacher model has a different view of the video clip with the student. Conceptually, the overpowered teacher causes a leakage [17] where our flow estimator can have access to the information of the target intermediate frame during training, and in the experiments section, we show that this kind of data (target) leakage is beneficial to the training of our whole system.

3.4. Implement Details

Supervisions. Given a pair of consecutive frames, I_0, I_1 , our training loss \mathcal{L} is a linear combination of the reconstruction loss \mathcal{L}_{rec} , adapted census loss [22] \mathcal{L}_{cen} and leakage distillation loss \mathcal{L}_{dis} as defined in section 3.3:

$$\mathcal{L} = \mathcal{L}_{rec} + \lambda_c \mathcal{L}_{cen} + \lambda_d \mathcal{L}_{dis}, \quad (4)$$

where we set $\lambda_c = 1$ and $\lambda_d = 0.01$.

The reconstruction loss \mathcal{L}_{rec} models the reconstruction quality of the intermediate frame. We denote the synthesized frame by \hat{I}_t and the ground-truth frame by I_t^{GT} . The reconstruction loss has the formulation of :

$$\mathcal{L}_{rec} = \|\hat{I}_t - I_t^{GT}\|_1. \quad (5)$$

As the brightness constancy constraint is often violated in realistic situations, census loss is widely used in unsupervised optical flow estimation [15] methods to address the illumination changes. We adopt the census loss from unsupervised optical flow learning [22, 15] to robustly handle the illumination changes between consecutive frames. The census loss is defined as the soft Hamming distance on census-transformed [38] image patches. We optimize the census loss \mathcal{L}_{cen} between census-transformed \hat{I}_t and I_t^{GT} with the width of patches as 9.

Training dataset. We use Vimeo90K (Triplet) dataset [37] to train our model. The Vimeo90K dataset has 51,312 triplets for training, where each triplet contains three consecutive video frames with a resolution of 256×448 . We randomly augment the training data by horizontal and vertical flipping and temporal order reversing during training. We crop every training example to a 224×224 patch. In the benchmark experiment of inter-frame interpolation, we train RIFE to predict the middle frame given the frames on both sides.

Training strategy. We train our system from scratch on the Vimeo90K training set. An official LiteFlowNet [11] pre-trained on the FlyingChairs [8] and FlyingThings3D [12] datasets is used as the overpowered teacher in the leakage distillation.

Our model is optimized by AdamW [20] with weight decay 10^{-4} for 300 epochs on the Vimeo90K training set. Our training uses a batch size of 48. We gradually reduce the learning rate from 10^{-4} to 0 using cosine annealing during the whole training process. Our pipeline is implemented in PyTorch. We train RIFE on four NVIDIA TITAN X (Pascal) GPUs for about 15 hours. The preprocess needs 2 hours in one GPU, and different models can use the same preprocess results.

4. Experiments

In this section, we conduct several experiments to validate our method. We first introduce the benchmarks for evaluation. Then we provide variants of our models with different computational costs to meet different needs in section 4.2. We compare our models with representative state-of-the-art methods, both quantitatively and visually, in section 4.3. An ablation study in section 4.4 is carried out to analyze our design of IFNet and the proposed leakage distillation loss. Finally, we show the capability of generating multiple frames using our models in section 4.5.

4.1. Benchmarks and Evaluation Metrics

We evaluate our model on four benchmarks, including Middlebury [1], UCF101 [31], Vimeo90K [37] and HD [3]. Following previous work, we train our models on the Vimeo90K training dataset and directly test it on all these benchmarks.

Middlebury. The Middlebury (M.B.) benchmark [1] is widely used to evaluate VFI methods. The image resolution in this dataset is around 640×480 . We report the average IE of the Middlebury-OTHER set.

Vimeo90K. There are 3,782 triplets in the Vimeo90K test set [37]. The image resolution in this dataset is 448×256 .

UCF101. The UCF101 dataset [31] contains videos with a large variety of human actions. There are 379 triplets with a resolution of 256×256 .

HD. Bao *et al.* [3] collect 11 high-resolution videos for evaluation. The HD benchmark consists of four 1080p, three 720p and four 1280×544 videos. The motions in this benchmark are larger than other benchmarks. Following the author of HD benchmark, we use the first 100 frames of each video for evaluation.

We measure the peak signal-to-noise ratio (PSNR), structural similarity (SSIM), and interpolation error (IE) for quantitative evaluation. All the methods are tested on an NVIDIA TITAN X (Pascal) GPU. We calculate the average

Table 2: **Quantitative comparisons on the UCF101 [31], Vimeo90K [37], Middlebury-OTHER set [1], and HD benchmarks [3].** The numbers in **red** and **blue** represent the best and second-best performance. We report the interpolation runtime for a single 640×480 video frame. Some methods are unable to run on 1080p videos due to exceeding the 12 gigabytes of memory available on our graphics card (denoted as “OOM”).

Method	# Parameters (Million)	Runtime (ms)	UCF101 [31]		Vimeo90K [37]		M.B. [1]	HD [3]
			PSNR	SSIM	PSNR	SSIM	IE	PSNR
DVF [19]	1.6	80	34.12	0.963	31.54	0.946	4.04	-
SuperSloMo [13, 7]	19.8	52	34.75	0.968	33.15	0.966	2.28	-
TOFlow [37]	1.1	72	34.58	0.967	33.73	0.968	2.15	29.37
SepConv [27]	21.6	51	34.78	0.967	33.79	0.970	2.27	30.87
MEMC-Net [3]	70.3	120(401) [†]	35.01	0.968	34.29	0.970	2.12	31.39
DAIN [2]	24.0	130(436) [†]	35.00	0.968	34.71	0.976	2.04	31.64(OOM) [†]
CAIN [7]	42.8	38	34.98	0.969	34.65	0.973	2.28 [‡]	31.77
SoftSplat [25]	7.7	135	35.39	0.970	36.10	0.980	1.81	-
BMBC [28]	11.0	1580	35.15	0.969	35.01	0.976	2.04	OOM
DSepConv [6]	21.8	236	35.08	0.969	34.73	0.974	2.03	OOM
EDSC [5]	8.9	46	35.13	0.968	34.84	0.975	2.02	31.59
RIFE (Ours)	9.8	16	35.25	0.969	35.51	0.978	1.96	31.99
RIFE-Large (Ours)	20.9	72	35.29	0.969	36.10	0.980	1.94	32.14

[†]: copy from [2], we compile released models and get three times slower.

[‡]: get 2.72 using officially released model.

Table 3: **Increase model complexity by adjusting model size parameters.** C denotes the multiplier for the number of channels, and F denotes the resolution multiplier. $2F$ represents removing the first downsampling layer of IFNet and the first one of FusionNet. The parameter setting of RIFE-Large is $1.5C2F$.

Scale Setting	RIFE	$1.5C$	$2F$	RIFE-Large
UCF101 PSNR	35.24	35.26	35.30	35.29
Vimeo90K PSNR	35.51	35.76	35.95	36.10
M.B. IE	1.96	1.96	1.94	1.94
HD PSNR	31.99	32.04	31.91	32.14
# Parameters*	9.8M	20.9M	9.8M	20.9M
Runtime*	35ms	50ms	126ms	234ms
Complexity*	200G	460G	790G	1780G

*: average runtime of 720p frames ($batchsize = 1$)

GPU process time for 100 runs after a warm-up process of 100 runs.

4.2. Model Scaling

We provide several models with different computation overheads and performance to meet different needs by model scaling. We introduce two hyper-parameters following [10]: width multiplier and resolution multiplier. Upon our base model RIFE, we apply a 1.5 width multiplier on the number of channels uniformly at each layer to produce a model named RIFE- $1.5C$. Meanwhile, we can remove a downsample layer from the headers of IFNet and Fusion-

Net, which doubles the feature map’s resolution that produces a model named RIFE- $2F$. Together, we can combine these two modifications to produce a model named RIFE-Large ($1.5C2F$). The performance and runtime for these models is reported in Table 3 and depicted in Figure 1. We show that our model is flexible, and simply increasing model capacity can effectively improve model performance. When RIFE processes 720p videos in parallel ($batchsize = 4$), the total runtime can further drop to half.

4.3. Comparisons with Previous Methods

We report the performance on the benchmarks mentioned above in Table 2. These methods are officially trained on Vimeo90K dataset except for DVF [19] and SuperSloMo [13]. RIFE runs considerably faster than other methods with comparable performance. Meanwhile, RIFE needs only 3.1 gigabytes of GPU memory to process 1080p videos, while some algorithms exceed 12 gigabytes. We get a larger version of our model (RIFE-Large) by simple model scaling, which runs about two times faster than the previous state-of-the-art method SoftSplat [25] with comparable performance. We provide a visual comparison of video clips with large motions from the Vimeo90K testing set in Figure 6, where SepConv [27] and DAIN [2] produce ghosting artifacts, and CAIN [7] causes missing-parts artifacts. Overall, our method can produce more reliable results.



Figure 6: **Qualitative comparison on Vimeo90K [37] testing set.** We cut out the objects according to the green boxes and zoom in the results [7]. While other methods cause various artifacts, our method produces best effects on the moving objects.

Table 4: **Ablation study on losses, intermediate flow estimation, and fusion process.**

Setting	Vimeo90K PSNR	M.B. IE	Runtime ms (720p)
w/o \mathcal{L}_{dis} and \mathcal{L}_{cen}	34.62	2.37	34
w/o \mathcal{L}_{dis}	34.89	2.29	34
w/o \mathcal{L}_{cen}	35.38	1.99	34
RIFE	35.51	1.96	34
linear combination [13]	34.58	2.25	118
CNN model	34.89	2.15	121
reversal layer [36]	35.24	2.06	232
RIFE (IFNet)	35.51	1.96	34
w/o fusion map	34.97	2.23	34
w/o residual	35.03	2.19	34
w/o context extractor	35.28	2.00	30
RIFE	35.51	1.96	34

4.4. Ablation Study

We design an ablation study on losses, intermediate flow estimation, and fusion process, shown in Table 4. These experiments use the same hyper-parameter setting and evaluation on Vimeo90K [37] and MiddleBury [1] benchmark.

Ablation on the losses. To analyze the contributions of adapted census loss \mathcal{L}_{cen} and leakage distillation loss \mathcal{L}_{dis} , we train RIFE models from scratch without these losses. We show that these two losses can improve the performance of RIFE, especially \mathcal{L}_{dis} . We also notice that the training of the model will become very unstable without \mathcal{L}_{dis} .

IFNet vs. flow reversal. To demonstrate the effectiveness of IFNet, we compare it with previous intermediate flow estimation methods used in SuperSlomo [13] and EQVI [18]. Specifically, we use PWC-Net [32] with officially pre-trained parameters to estimate the bi-directional flows. Then we implement three flow reversal methods, including linearly combination [13], using a hidden convolutional layer with 128 channels, and the flow reversal method from EQVI [18] consists of a reversal layer and an U-Net filter. The PWC-Net and flow reversal modules are jointly trained with our fusion process. As shown in Table 4, IFNet is more efficient and accurate in estimating intermediate flows leads to better interpolation performance.

Ablation on the fusion process. To study the fusion process design, we remove the fusion map and residual term, resulting in blurry results and performance degradation. Moreover, we verify the context extractor can improve performance with a small computational overhead.

4.5. Generating Multiple Frames

To interpolate multiple intermediate frames at different time $t \in (0, 1)$, we can apply RIFE recursively. Specifically, given any two consecutive input frames I_0, I_1 , we apply RIFE once to get intermediate frame $\hat{I}_{0.5}$ at $t = 0.5$. We feed I_0 and $\hat{I}_{0.5}$ to get $\hat{I}_{0.25}$, and we can repeat this process recursively to get the multiple frames. To demonstrate this ability, we provide the visual results for $2\times, 4\times, 8\times$ settings on images with large motions from the Vimeo90K testing set in Figure 7. We observe that RIFE successfully

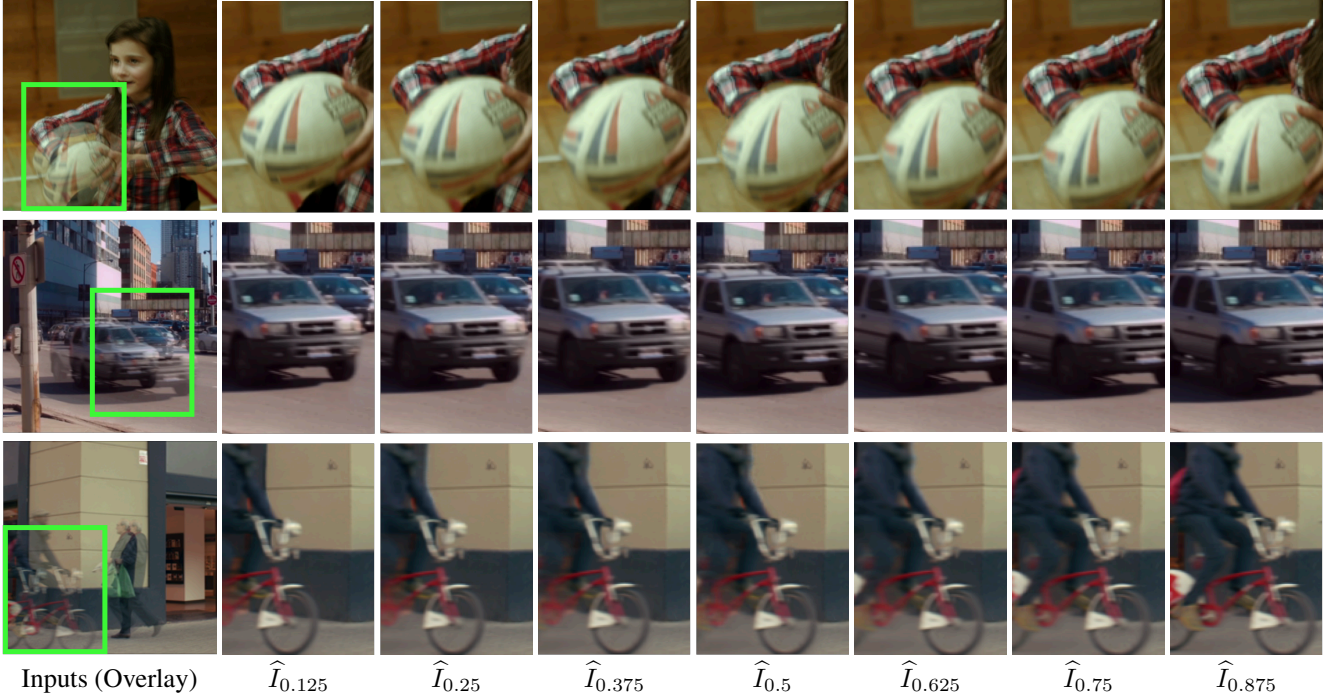


Figure 7: **Interpolating multiple frames on the Vimeo90K testing dataset by applying RIFE recursively.** We cut out the moving objects according to the green boxes and zoom in the results. RIFE provides smooth and continuous motions.

Table 5: **Quantitative evaluation for $8\times$ interpolation on the HD benchmark [3].** Some methods [2, 28, 5] can support interpolation at arbitrary time, while others [7, 6] can be only applied recursively to get multiple frames.

Method	Recursion	544×1280	720p	1080p
DAIN [2]	✓	19.32	28.81	OOM
DAIN [2]	-	19.03	27.97	OOM
CAIN [7]	✓	18.37	28.31	24.71
BMBC [28]	✓	18.16	26.70	OOM
BMBC [28]	-	17.12	19.60	OOM
DSeconv [6]	✓	16.80	19.57	OOM
EDSC _s [5]	✓	18.15	28.39	24.22
EDSC _m [5]	-	18.89	27.03	25.49
RIFE (Ours)	✓	18.89	28.83	24.96

produces smooth and continuous motions.

To provide a quantitative comparison for $8\times$ interpolation, we further extract $8k^{th}$ ($0 \leq 8k < 100$) of every video from HD benchmark [3] and use them to interpolate other frames. We divide the HD benchmark into three subsets with different resolution to test these methods. We show the quantitative PSNR between generated frames and frames of the origin videos in Table 5. Note that DAIN [2], BMBC [28] and EDSC_m [6] can generate a frame at an arbitrary time between the input ones. But they do not show obvious advantages over recursive frame interpolation methods. Among these methods, DAIN has the best results.

However, DAIN’s speed is relatively slower than CAIN [7] and RIFE. Overall, RIFE has stable performance and low overhead in the $8\times$ interpolation scenario.

5. Discussion and Conclusion

We show that we can get large efficiency and performance improvement by combining proper representations and supervisions. However, our work has some limitations. First, RIFE does not support directly generating frames at arbitrary time. Using additional training data and following techniques proposed in SuperSlomo [13], QVI [36], and BMBC [28] may be a feasible approach. Second, RIFE focuses on only using two input frames while multi-frame input is proven to improve the effect of frame interpolation [36, 18, 16]. Third, many previous papers point out that SSIM and PSNR are not consistent with human subjective perception [26, 25], and optimizing perceptual loss [14] and LPIPS [39] may be essential for training a practical model for video processing.

In this work, we develop an efficient and flexible algorithm for VFI, named RIFE. With the more accurate flow estimation and our fusion process, RIFE can effectively process videos of different resolution and interpolate multiple frames between two input frames. The impressive results of the proposed method shed light for future research on realtime flow-based interpolation methods.

References

- [1] baker2011database. A database and evaluation methodology for optical flow. In *International Journal of Computer Vision (IJCV)*, 2011. 5, 6, 7
- [2] Wenbo Bao, Wei-Sheng Lai, Chao Ma, Xiaoyun Zhang, Zhiyong Gao, and Ming-Hsuan Yang. Depth-aware video frame interpolation. In *Proceedings of the IEEE Conference on Computer Vision and Pattern Recognition (CVPR)*, 2019. 1, 2, 3, 4, 6, 8
- [3] Wenbo Bao, Wei-Sheng Lai, Xiaoyun Zhang, Zhiyong Gao, and Ming-Hsuan Yang. Memc-net: Motion estimation and motion compensation driven neural network for video interpolation and enhancement. *IEEE Transactions on Pattern Analysis and Machine Intelligence (IEEE TPAMI)*, 2018. 1, 5, 6, 8
- [4] Ting Chen, Simon Kornblith, Kevin Swersky, Mohammad Norouzi, and Geoffrey Hinton. Big self-supervised models are strong semi-supervised learners. *arXiv preprint arXiv:2006.10029*, 2020. 5
- [5] Xianhang Cheng and Zhenzhong Chen. Multiple video frame interpolation via enhanced deformable separable convolution. *arXiv preprint arXiv:2006.08070*, 2020. 1, 2, 6, 8
- [6] Xianhang Cheng and Zhenzhong Chen. Video frame interpolation via deformable separable convolution. In *Proceedings of the Association for the Advancement of Artificial Intelligence (AAAI)*, 2020. 1, 2, 6, 8
- [7] Myungsub Choi, Heewon Kim, Bohyung Han, Ning Xu, and Kyoung Mu Lee. Channel attention is all you need for video frame interpolation. In *Proceedings of the Association for the Advancement of Artificial Intelligence (AAAI)*, 2020. 1, 2, 6, 7, 8
- [8] Alexey Dosovitskiy, Philipp Fischer, Eddy Ilg, Philip Hausser, Caner Hazirbas, Vladimir Golkov, Patrick Van Der Smagt, Daniel Cremers, and Thomas Brox. FlowNet: Learning optical flow with convolutional networks. In *Proceedings of the IEEE International Conference on Computer Vision (ICCV)*, 2015. 2, 5
- [9] Kaiming He, Xiangyu Zhang, Shaoqing Ren, and Jian Sun. Delving deep into rectifiers: Surpassing human-level performance on imagenet classification. In *Proceedings of the IEEE International Conference on Computer Vision (ICCV)*, 2015. 4
- [10] Andrew G Howard, Menglong Zhu, Bo Chen, Dmitry Kalenichenko, Weijun Wang, Tobias Weyand, Marco Andreetto, and Hartwig Adam. Mobilenets: Efficient convolutional neural networks for mobile vision applications. *arXiv preprint arXiv:1704.04861*, 2017. 6
- [11] Tak-Wai Hui, Xiaoou Tang, and Chen Change Loy. Lite-flownet: A lightweight convolutional neural network for optical flow estimation. In *Proceedings of the IEEE Conference on Computer Vision and Pattern Recognition (CVPR)*, 2018. 2, 4, 5
- [12] Eddy Ilg, Nikolaus Mayer, Tonmoy Saikia, Margret Keuper, Alexey Dosovitskiy, and Thomas Brox. FlowNet 2.0: Evolution of optical flow estimation with deep networks. In *Proceedings of the IEEE Conference on Computer Vision and Pattern Recognition (CVPR)*, 2017. 2, 4, 5
- [13] Huaizu Jiang, Deqing Sun, Varun Jampani, Ming-Hsuan Yang, Erik Learned-Miller, and Jan Kautz. Super slo-mo: High quality estimation of multiple intermediate frames for video interpolation. In *Proceedings of the IEEE Conference on Computer Vision and Pattern Recognition (CVPR)*, 2018. 1, 2, 3, 4, 6, 7, 8
- [14] Justin Johnson, Alexandre Alahi, and Li Fei-Fei. Perceptual losses for real-time style transfer and super-resolution. In *Proceedings of the European Conference on Computer Vision (ECCV)*, 2016. 8
- [15] Rico Jonschkowski, Austin Stone, Jonathan T Barron, Ariel Gordon, Kurt Konolige, and Anelia Angelova. What matters in unsupervised optical flow. In *Proceedings of the European Conference on Computer Vision (ECCV)*, 2020. 2, 5
- [16] Tarun Kalluri, Deepak Pathak, Manmohan Chandraker, and Du Tran. Flavr: Flow-agnostic video representations for fast frame interpolation. *arXiv preprint arXiv:2012.08512*, 2020. 8
- [17] Shachar Kaufman, Saharon Rosset, Claudia Perlich, and Ori Stitelman. Leakage in data mining: Formulation, detection, and avoidance. *ACM Transactions on Knowledge Discovery from Data (TKDD)*, 6(4):1–21, 2012. 5
- [18] Yihao Liu, Liangbin Xie, Li Siyao, Wenxiu Sun, Yu Qiao, and Chao Dong. Enhanced quadratic video interpolation. In *Proceedings of the European Conference on Computer Vision (ECCV)*, 2020. 1, 2, 3, 7, 8
- [19] Ziwei Liu, Raymond A Yeh, Xiaoou Tang, Yiming Liu, and Aseem Agarwala. Video frame synthesis using deep voxel flow. In *Proceedings of the IEEE International Conference on Computer Vision (ICCV)*, 2017. 2, 6
- [20] Ilya Loshchilov and Frank Hutter. Fixing weight decay regularization in adam. 2018. 5
- [21] Kunming Luo, Chuan Wang, Shuaicheng Liu, Haoqiang Fan, Jue Wang, and Jian Sun. Upflow: Upsampling pyramid for unsupervised optical flow learning. *arXiv preprint arXiv:2012.00212*, 2020. 2
- [22] Simon Meister, Junhwa Hur, and Stefan Roth. UnFlow: Unsupervised learning of optical flow with a bidirectional census loss. In *Proceedings of the Association for the Advancement of Artificial Intelligence (AAAI)*, 2018. 2, 5
- [23] Simone Meyer, Oliver Wang, Henning Zimmer, Max Grosse, and Alexander Sorkine-Hornung. Phase-based frame interpolation for video. In *Proceedings of the IEEE Conference on Computer Vision and Pattern Recognition (CVPR)*, 2015. 2
- [24] Simon Niklaus and Feng Liu. Context-aware synthesis for video frame interpolation. In *Proceedings of the IEEE Conference on Computer Vision and Pattern Recognition (CVPR)*, 2018. 1
- [25] Simon Niklaus and Feng Liu. Softmax splatting for video frame interpolation. In *Proceedings of the IEEE Conference on Computer Vision and Pattern Recognition (CVPR)*, 2020. 1, 2, 4, 6, 8
- [26] Simon Niklaus, Long Mai, and Feng Liu. Video frame interpolation via adaptive convolution. In *Proceedings of the*

- IEEE Conference on Computer Vision and Pattern Recognition (CVPR)*, 2017. 2, 8
- [27] Simon Niklaus, Long Mai, and Feng Liu. Video frame interpolation via adaptive separable convolution. In *Proceedings of the IEEE International Conference on Computer Vision (ICCV)*, 2017. 1, 2, 6
 - [28] Junheum Park, Keunsoo Ko, Chul Lee, and Chang-Su Kim. Bmbc: Bilateral motion estimation with bilateral cost volume for video interpolation. In *Proceedings of the European Conference on Computer Vision (ECCV)*, 2020. 1, 2, 6, 8
 - [29] Fitsum A Reda, Deqing Sun, Aysegul Dunder, Mohammad Shoeybi, Guilin Liu, Kevin J Shih, Andrew Tao, Jan Kautz, and Bryan Catanzaro. Unsupervised video interpolation using cycle consistency. In *Proceedings of the IEEE International Conference on Computer Vision (ICCV)*, 2019. 2
 - [30] Olaf Ronneberger, Philipp Fischer, and Thomas Brox. U-net: Convolutional networks for biomedical image segmentation. In *International Conference on Medical image computing and computer-assisted intervention (MICCAI)*, 2015. 2
 - [31] Khurram Soomro, Amir Roshan Zamir, and Mubarak Shah. UCF101: A dataset of 101 human actions classes from videos in the wild. *CoRR*, abs/1212.0402, 2012. 5, 6
 - [32] Deqing Sun, Xiaodong Yang, Ming-Yu Liu, and Jan Kautz. Pwc-net: Cnns for optical flow using pyramid, warping, and cost volume. In *Proceedings of the IEEE Conference on Computer Vision and Pattern Recognition (CVPR)*, 2018. 2, 4, 7
 - [33] Zachary Teed and Jia Deng. Raft: Recurrent all-pairs field transforms for optical flow. In *Proceedings of the European Conference on Computer Vision (ECCV)*, 2020. 2, 5
 - [34] Chao-Yuan Wu, Nayan Singhal, and Philipp Krahenbuhl. Video compression through image interpolation. In *Proceedings of the European Conference on Computer Vision (ECCV)*, 2018. 1
 - [35] Qizhe Xie, Minh-Thang Luong, Eduard Hovy, and Quoc V Le. Self-training with noisy student improves imagenet classification. In *Proceedings of the IEEE Conference on Computer Vision and Pattern Recognition (CVPR)*, 2020. 5
 - [36] Xiangyu Xu, Li Siyao, Wenxiu Sun, Qian Yin, and Ming-Hsuan Yang. Quadratic video interpolation. In *Advances in Neural Information Processing Systems (NIPS)*, 2019. 1, 2, 3, 7, 8
 - [37] Tianfan Xue, Baian Chen, Jiajun Wu, Donglai Wei, and William T Freeman. Video enhancement with task-oriented flow. In *International Journal of Computer Vision (IJCV)*, 2019. 1, 5, 6, 7
 - [38] Ramin Zabih and John Woodfill. Non-parametric local transforms for computing visual correspondence. In *Proceedings of the European Conference on Computer Vision (ECCV)*, 1994. 5
 - [39] Richard Zhang, Phillip Isola, Alexei A Efros, Eli Shechtman, and Oliver Wang. The unreasonable effectiveness of deep features as a perceptual metric. In *Proceedings of the IEEE Conference on Computer Vision and Pattern Recognition (CVPR)*, 2018. 8